Strain-Induced Porosity during Cogging of Extra-Low Interstitial Grade Ti-6Al-4V

S. Tamirisakandala, Steve C. Medeiros, William G. Frazier, and Y.V.R.K. Prasad

(Submitted 7 June 2000)

The phenomenon of strain-induced porosity (SIP) in extra-low interstitial (ELI) grade Ti-6Al-4V with a transformed β starting microstructure is investigated to understand its origin during α-β cogging. For this purpose, the constitutive behavior of the material is coupled with finite-element method (FEM) simulations of the cogging process. Two distinct types of SIP relevant to cogging speeds and temperatures, *viz.*, shear cracking and void nucleation, are identified. While the former occurs at the prior β grain boundaries below 825 °C, the latter occurs at the prior colony boundaries when the deformation temperature is close to the β transus. The FEM simulations have shown that deformation conditions existing in the midregion of the billet are favorable for void nucleation. The mechanism of void growth in the presence of tensile residual stress and temperature during resoaking is modeled using the Cocks-Ashby coupled growth model. Repeated cogging and resoaking steps cause multiplication of void population in large numbers. To avoid both types of defects in any region of the billet, a practical solution has been developed by introducing a differential temperature profile from the surface to the center, and the validity of the proposed scheme is verified with FEM heat-transfer simulations.

Keywords cogging, FEM analysis, hot working, strain-induced porosity, Ti-6Al-4V

1. Introduction

Ti-6Al-4V (Ti-6-4) is the most widely used titanium alloy in aerospace applications due to its attractive mechanical properties. This alloy is available in two grades, which are distinguished by the interstitial impurity (primarily oxygen) content.[1] The extra-low interstitial (ELI) grade, which contains 0.10 to 0.13 wt.% oxygen, is used for fracture critical applications such as bulkheads, because it possesses a 30% higher fracture toughness than the regular (or commercial) grade, which contains 0.16 to 0.20 wt.% oxygen.[2] Hot working operations involving ingot breakdown and conversion are essential steps in the manufacture of Ti-6-4 mill products. Ingot breakdown consists of upset forging and side pressing in the β-phase field (above the β transus) followed by air cooling, which produces a transformed β (Widmanstätten) microstructure consisting of lamellar colonies within large prior β grains. The microstructure is converted from lamellar to fine equiaxed $\alpha + \beta$ by using a cogging process in the α-β phase field (below the β transus). Cogging is a simple open-die forging between flat dies, which is used to reduce the cross-sectional area by a series of short bites along the length of the ingot and is performed using slow speed machines such as hydraulic presses. In view of the relatively large section size of the ingot (*e.g.*, 1000 mm thick), strain penetration through its thickness is not fully achievable in a single step. Therefore, cogging is performed using several cycles of limited deformation and reheating. Temperature is one of the most important parameters in the design of the conversion sequence for obtaining the required final microstructure. It is important to note that, if the process schedule used for regular grade conversion is used for cogging ELI grade, the working temperature will be close to its β transus, because the transus in ELI grade is lower by about 35 °C than that of the regular grade.

Development of strain-induced porosity (SIP) under certain thermomechanical conditions is a serious problem during Ti-6-4 ingot conversion.[3–8] The formation of SIP in the cogged billets is highly unacceptable for further processing, and, once formed, it can only be sealed by expensive and time-consuming methods such as hot-isostatic pressing (HIP). The general manifestation of SIP is in the form of wedge cracks or pores at the prior β grain boundaries. To explain this phenomenon, Semiatin *et al.*[5,6] studied the cavitation behavior during hot tension and forging using cavity initiation and coalescence models to develop a criterion based on the tensile work. Seshacharyulu *et al.*[7,8] characterized the hot deformation behavior of regular and ELI grade Ti-6-4 with transformed β starting microstructures over wide temperature and strain rate ranges and established the limits for prior β boundary cracking. These studies revealed that SIP voids also nucleate within the interiors of the β grains, and this type of SIP is found to be specific to ELI grade.[9] However, results obtained from materials modeling have to be integrated with the state-of-stress information during cogging in order to understand the mechanism of SIP.

The objectives of this study are (1) to obtain detailed insight into the origin and characteristics of SIP during conversion of ELI grade Ti-6-4 and (2) to develop a practical solution for avoiding SIP formation in the cogged billets. This study will be valuable not only for improving and optimizing the process design but also for avoiding costly repair processes such HIP. To meet the above objectives, the results obtained using materials

S. Tamirisakandala, Steve C. Medeiros, William G. Frazier, and **Y.V.R.K. Prasad,** Materials Process Design Branch (AFRL/MLMR), Materials and Manufacturing Directorate, Air Force Research Laboratory, Wright-Patterson Air Force Base, OH 45433-7746. Contact e-mail: sesh@australinc.com.

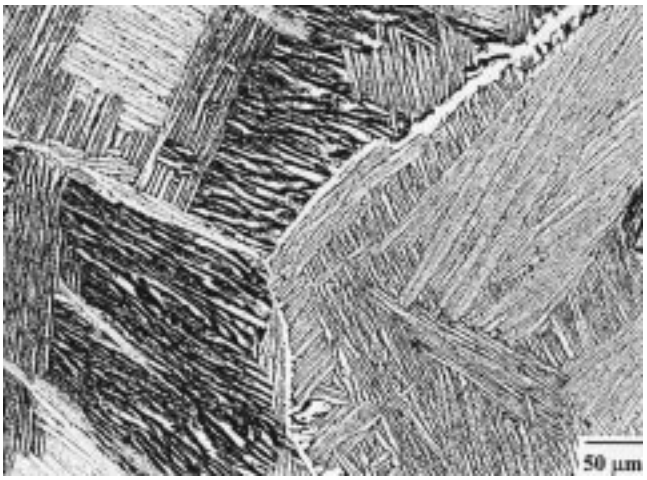

Fig. 1 Starting microstructure of ELI Ti-6Al-4V used for testing

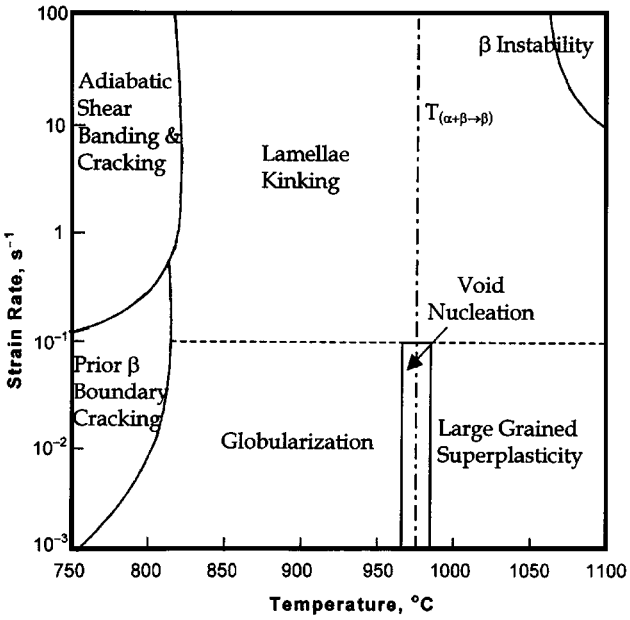

Fig. 2 Microstructural mechanism map for ELI Ti-6Al-4V over wide temperature and strain rate ranges

modeling techniques in an earlier study[8] are coupled with finite-element method (FEM) analysis of the cogging sequence.

2. Experimental

2.1 Material

The ELI grade Ti-6-4 used in this study had the following composition (weight percent): Al-6.04, V-3.91, O-0.13, Fe-0.08, and N-0.008. The β transus for this material is approximately 975 °C. The material was taken from a billet that was subjected to a few steps of β cogging followed by water quenching. The starting microstructure is shown in Fig. 1 and consists of lamellar α (transformed β) colonies in large prior β grains of about 2 to 3 mm, a grain boundary α layer of 5 μm thickness, and a very thin β layer in between the colony boundaries and grain boundary α.

2.2 Hot Compression Testing

For establishing constitutive equations and processing maps, isothermal hot compression tests were conducted in the temperature range 750 to 1100 °C at 50 °C intervals and constant true strain rate range 0.001 to 100 s^{-1} at order of magnitude intervals. Cylindrical specimens of 10 mm diameter and 15 mm height were used. Detailed testing procedures can be found in Ref 8. The specimens were deformed to half the height in each case to impose a true strain of about 0.7 and were air-cooled to room temperature after deformation. Deformed specimens were sectioned parallel to the compression axis, and the cut surface was prepared for metallographic examination using standard techniques. The specimens were etched with Kroll's reagent, and optical micrographs were recorded.

2.3 Hot Tensile Testing

Hot tensile tests were conducted in the temperature range 800 to 1100 °C at a nominal strain rate of 0.01 s^{-1} (constant actuator speed of 0.25 mm s^{-1}). Cylindrical specimens of 25 mm gauge length and 4 mm gauge diameter were used for this purpose. They were coated with glass lubricant for environmental protection. The specimens were pulled to fracture, and total elongation as a function of temperature was recorded.

3. Results and Discussion

3.1 Constitutive Behavior

On the basis of flow stress data obtained in the ranges 750 to 1100 °C and 0.001 to 100 s^{-1} for ELI Ti-6-4 with lamellar starting microstructure, a processing map has been developed, and the atomistic mechanisms of hot working have been identified and validated with detailed microstructural observations.[8] The constitutive behavior of the material during hot deformation is summarized in the form of a microstructural mechanism map shown in Fig. 2. The material exhibits the following mechanisms.

A. Prior β Boundary Cracking. In the lower α-β temperature range (<825 °C), microstructural observations revealed that cracks occur at the prior β boundaries during deformation and the majority of them are found in the bulge regions of compressed specimens along the boundaries oriented at about 45° to the compression axis. The representative microstructure of a specimen deformed in this regime at 800 °C/0.01 s^{-1} is shown in Fig. 3. This type of cracking has been identified as "shear" cracking, and its detailed microstructural mechanism is discussed elsewhere.[6,8] In simple terms, under a resolved shear stress, prior β boundaries oriented at ~45° with respect to the compression axis slide along the thin soft β layer in between the Widmanstätten colonies and the grain boundary α layer and produce stress concentrations at the boundaries/triple junctions. Due to specific crystallographic orientation relationships, the colonies are harder than the grain boundary α layer, and hence, the stress concentrations can be relieved only by

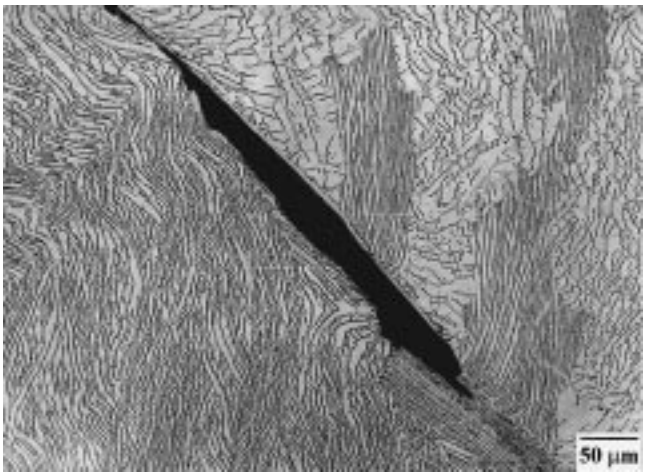

Fig. 3 Microstructure of ELI Ti-6Al-4V specimen deformed at 800 °C and 0.01 s^{-1} exhibiting cracking at the prior β grain boundary. The compression axis is vertical

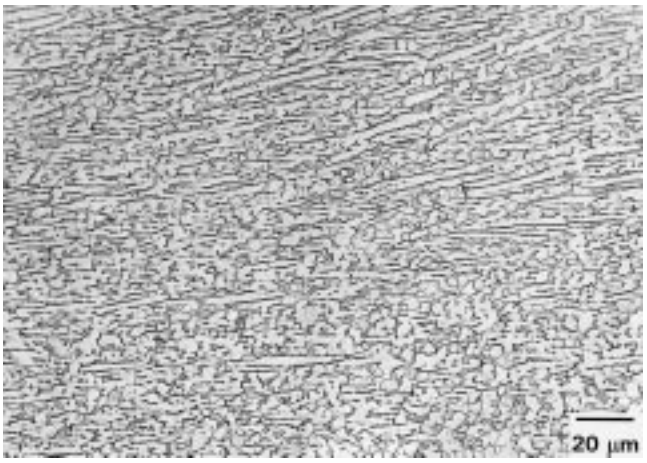

Fig. 4 Microstructure of ELI Ti-6Al-4V specimen deformed at 900 °C and 0.001 s^{-1} exhibiting globularization of lamellar structure

the softening of grain boundary α (*e.g.*, by dynamic recrystallization) at rates at least as fast as the buildup of boundary stress. If the stress concentrations are not relieved by the deformation of adjacent grain boundary α phase, cracks form along the interface and these cracks can easily open under a tensile state of stress.

B. Globularization. In the intermediate α-β temperature range (825 to 950 °C), the microstructures of deformed specimens indicated a significant change in the morphology of α phase from lamellar to equiaxed. Typical microstructure of a specimen deformed at 900 °C/0.001 s^{-1} is shown in Fig. 4, which exhibits globularization of the lamellar structure. The extent of globularization and the globule size are less at lower temperatures and higher strain rates. The variation of the total tensile elongation with temperature for ELI Ti-6-4 at a nominal strain rate of 0.01 s^{-1} is shown in Fig. 5. The curve exhibits a peak (~55%) in the α-β range at about 925 °C, which is the optimum temperature for globularization. The process of

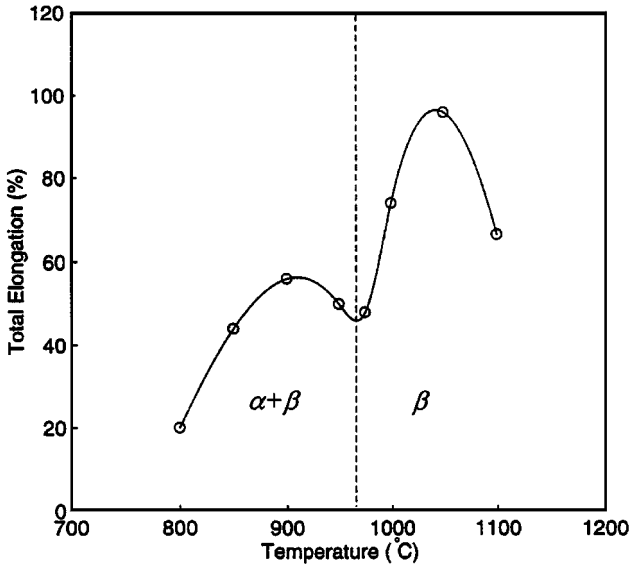

Fig. 5 Variation of tensile ductility with temperature for ELI Ti-6Al-4V at a nominal strain rate of 0.01 s^{-1}

globularization assumes considerable importance in the conversion, because this step produces the desired fine-grained equiaxed α-β microstructures for further processing into finished shapes.

C. Large Grained Superplasticity of β. In the β range, the ductility curve (Fig. 5) exhibits high elongations with a peak value of ~100% at 1050 °C even at strain rates as fast as 0.01 s^{-1}. On the basis of high elongation and moderate strain rate sensitivity (~0.3), the β deformation mechanism is identified[8] as large grained superplasticity (LGSP), which has been observed in several other materials such as β titanium alloys, β brasses, and aluminides.[10] The mechanism of LGSP is associated with the sliding of prior colony boundaries and simultaneous accommodation by diffusional flow. The sliding process contributes significantly to the total strain if the stress at their triple junctions is accommodated by diffusional flow, which is possible at higher temperatures (*e.g.*, 1050 °C).

D. Void Nucleation. The mechanism of superplasticity can cause nucleation of voids on grain boundaries as a result of incomplete accommodation of grain boundary sliding. The local minimum in the ductility curve (Fig. 5) around the transus (~975 °C) indicates that this is indeed the case in ELI Ti-6-4. At temperatures close to the transus, β diffusional flow is too slow to relax the stress concentration at triple junctions produced by the prior colony boundary sliding, and therefore, a distinct possibility of void formation within the prior β grains exists instead of LGSP. Void nucleation can occur only at strain rates lower than about 0.1 s^{-1}, because the boundary sliding ceases at higher strain rates. It is important to note that this type of intragranular SIP is much different from the previously discussed prior β boundary cracking, which essentially occurs at temperatures below 825 °C.

E. Flow Instabilities. The material exhibits large regimes of flow instability at higher strain rates (>0.1 s^{-1}), which are manifested as adiabatic shear banding and lamellae kinking in the α-β range and flow localization in the β range. Because the strain rates involved in slow speed cogging are generally

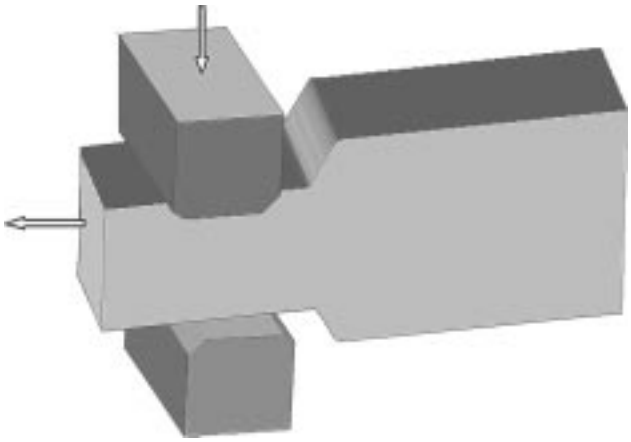

(**a**)

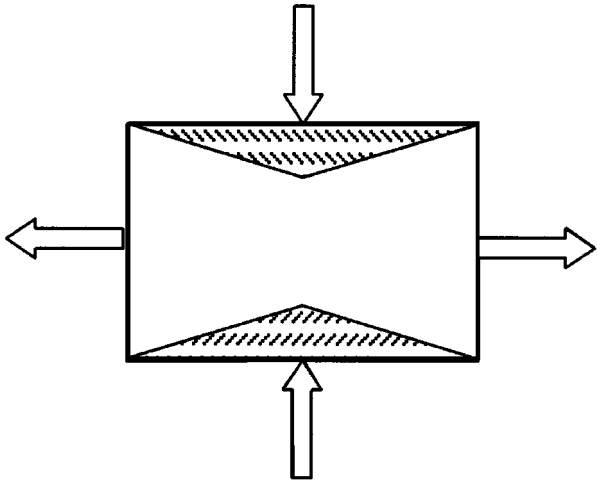

(**b**)

Fig. 6 Schematic illustrating (**a**) cogging process and (**b**) state of stress during cogging

below 0.1 s^{-1}, these microstructural defects are not expected to form in the cogged billets. The map (Fig. 2) clearly reveals that SIP, relevant to cogging speeds, is essentially of two types: prior β boundary cracking at lower temperatures and void nucleation near the β transus.

3.2 FEM Simulation of Cogging

With a view to understand the effect of state of stress on SIP formation, the mechanics of cogging were analyzed using finite-element simulations. Cogging can be considered as a plane-strain deformation process, and the state of stress in simplified terms is schematically shown in Fig. 6. Apart from the dead metal zone, it consists of compression in the normal direction and tension along the length of the billet. Two-dimensional FEM simulations of cogging bites have been conducted[11] using a large viscoplasticity FEM code ANTARES™ to evaluate the local stresses, strain rates, strains, and temperatures in the billet. The corrected flow stress data of ELI Ti-6-4 obtained in this investigation was input as constitutive equations into the FEM engine. The following thermophysical property data taken from Ref 1 were used: density = 4428 kgm^{-3}, specific heat = 970 J kg^{-1} K^{-1}, thermal conductivity = 21.5 Ns^{-1} K^{-1}, emissivity = 0.65, convection heat-transfer coefficient = 0.02 Ns^{-1} mm^{-1} $°C^{-1}$, coefficient of thermal expansion = 11 × 10^{-6} $°C^{-1}$, and Young's modulus = 55 GPa. An interfacial friction factor of 0.3 was used and the die speed was set to 4.2 mm/s. The simulations revealed that the stress state changes from compressive to tensile from the surface to the center, and a large tensile principal stress of 39 MPa exists in the midplane of the billet. The effective strain rate is found to vary between 0.15 s^{-1} on the surface to 0.05 s^{-1} in the midplane.

3.3 Void Nucleation and Growth during Cogging and Resoaking

Although microstructural modeling provided a detailed insight into the prior β boundary cracking type of SIP, it only indicated a possibility of void nucleation at higher temperatures. Microstructural observations of voids at the nucleation stage are difficult to make, and a significant requirement for void growth is the presence of a large local tensile stress.[12] These types of voids are referred to as "*r*-type" creep cavities in the literature.[13,14] Cocks and Ashby[13] developed detailed cavity growth models and formulated equations to obtain time and strain to fracture. In the early stages, cavity growth occurs by diffusional creep followed by power-law creep at later stages. The α-β cogging schedule generally practiced in industry is analyzed along with the state-of-stress information obtained from the FEM simulations to understand the origin of void formation at higher temperatures.

During cogging, the billets are heated to a uniform temperature (~960 °C) and are quickly transferred to the press in less than a minute. While the surface temperature drops during transfer and cogging, the midplane temperature remains unchanged due to large section size. The FEM simulations have shown that the midplane experiences a strain rate of 0.05 s^{-1}, which is ideal for void nucleation within the β grains at temperatures close to the transus. The simulations also revealed that a large tensile stress of 39 MPa, which is about half the flow stress of the alloy at 960 °C, locks up as residual stress in the midplane. Based on the Cocks-Ashby coupled growth model,[13] Raj[14] derived a simplified equation to estimate the minimum time required for cavity growth, which is given by

$$t_g = A \frac{kT}{\sigma_1 \Omega} \frac{\lambda^3}{(\delta D_b + \pi \lambda D_v)}$$

where A is a constant (6×10^{-3}), k is the Boltzmann's constant (1.38×10^{-23} J $mole^{-1}$), T is the absolute temperature, σ_1 is the maximum principal stress, λ is the void spacing, Ω is the atomic volume, δD_b is the boundary diffusion coefficient, and D_v is the volume diffusion coefficient. Substituting the values T = 1233 K, σ_1 = 39 MPa, $\Omega = 1.8 \times 10^{-29}$ m^3, λ = 50 μm (assumed), $\delta D_b = 1.89 \times 10^{-23}$ m^3 s^{-1}, and $D_v = 6.65 \times 10^{-14}$ m^2 s^{-1} in the above equation, the minimum time required for void growth is estimated to be about 30 min. This time is easily met during the resoaking step after cogging.

Since a cogging cycle consists of a number of cogging and resoaking steps, more and more voids nucleate in the midplane during cogging steps and their growth occurs during resoaking

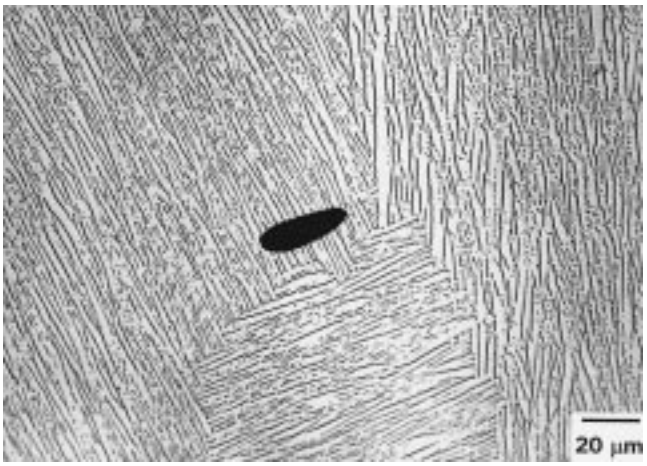

Fig. 7 Microstructure of a specimen taken from the center of a billet subjected to few α-β cogging and resoaking steps

periods. Void multiplication can result in significant porosity in the midregion of the billet at the end of the cogging cycle. Typical microstructure of a grown void observed in a specimen taken from the midregion of a billet subjected to a few α-β cogging and resoaking steps is shown in Fig. 7.

3.4 Differential Cogging Scheme

The microstructural mechanism map (Fig. 2) clearly indicates that the temperature and strain rate limits for the globularization (safe) region are set by the occurrence of damage processes on either side. When the temperature drops below 825 °C (which is possible on the surface regions of the billet being cogged), cracking at the prior β boundaries occurs. On the other hand, if the temperature is close to the transus (which occurs in the midregion of the billet), voids nucleate and grow in the presence of residual tensile stress and temperature during resoaking. These damage processes require a close control of temperature in the billet in order to avoid damaging microstructures in any region of the billet. Although a high temperature (~960 °C) in the surface region of the billet ensures avoidance of prior β cracking by compensating the heat loss during transfer, exposure to the surroundings and contact with colder dies, maintaining a lower midregion temperature (not greater than 940 °C), is essential for avoiding void nucleation and growth. Hence, avoidance of both the SIP defects requires a differential temperature profile from the surface to the center of the billet. Heat-transfer simulations using DEFORM™ FEM software[15] were conducted to check the feasibility of the temperature gradient concept.

The temperature distribution in one-quarter of the billet after soaking at 960 °C for 5 h is shown in Fig. 8(a). A differential temperature profile with 960 °C on the surface and 915 °C in the midregion of the billet can be observed. The temperature profile in the billet just before the start of cogging obtained by free air cooling of the billet for 1 min (assumed billet transfer time) is shown in Fig. 8(b). During transfer, the surface temperature drops to 875 °C, while the midregion still maintains at 915 °C. This differential profile ensures uniform globularized microstructure in the entire billet. Figure 8(b) also shows a

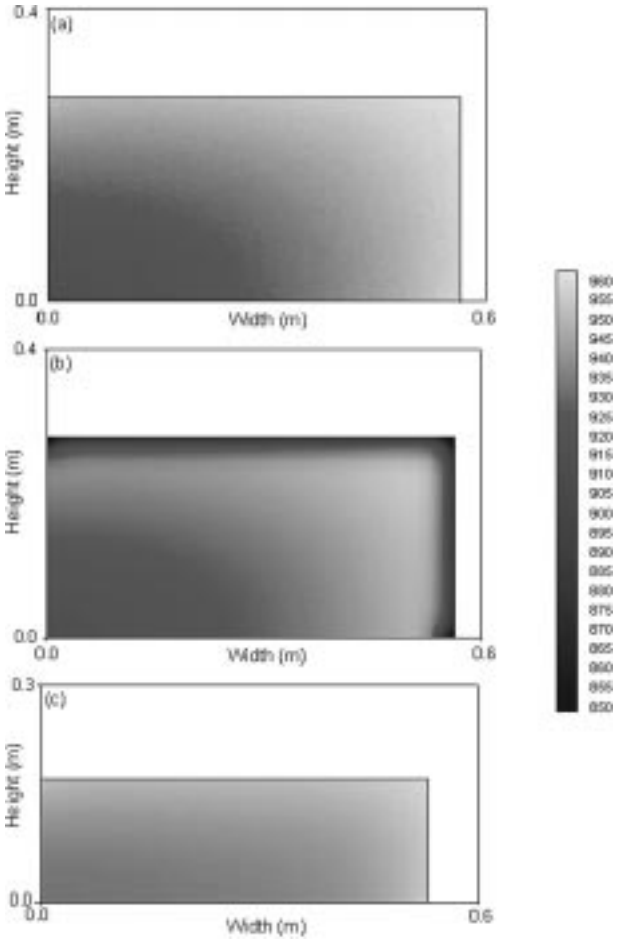

Fig. 8 Differential temperature profiles in one-quarter billet obtained from FEM heat-transfer simulations: (a) after 5 h soak at 960 °C, (b) at the beginning of cogging, and (c) after 30 min resoak of the cogged billet at 960 °C

region with temperature close to 960 °C near the surface, and it is likely that voids nucleate in this region during cogging. However, these voids will not grow during resoaking because of the compressive state of stress existing in this region.

As the cogging cycle is continued, the billet height reduces in each cogging step. This geometry change must be taken into account while designing the resoaking times for the avoidance of SIP at any stage of cogging. Heat-transfer simulations indicated that, while resoaking for 60 min is required in the early stages of cogging, 20 min resoaking is sufficient in the final stages for maintaining the differential temperature profile. The temperature variation after 30 min resoak of a reduced thickness billet is shown in Fig. 8(c). The profile reveals that, although it is not possible to obtain a differential profile similar to that in the large size billet, a safe profile can be maintained by reducing the resoaking time.

4. Summary and Conclusions

The origin of SIP during cogging of ELI grade Ti-6Al-4V with a transformed β starting microstructure has been examined

on the basis of constitutive behavior modeling and finite-element simulations of the cogging process. The SIP was found to be of two types: shear cracking at the prior β boundaries and void formation within the β grains. Shear cracking occurs on the surface layers of the billet when the temperature drops below 825 °C. Void nucleation occurs in the midregion of the billet during cogging when the temperature is close to the transus, and void growth occurs during resoaking by creep relaxation of the tensile residual stress locked in during cogging. Void multiplication occurs during repeated cogging and resoaking cycles. A solution to avoid both the defects has been developed by introducing a differential temperature in the billet with lower midplane temperature and higher surface temperature.

Acknowledgments

The authors thank Dr. James C. Malas for many stimulating discussions. One of the authors (YVRKP) is thankful to the National Research Council (United States) for awarding him an associateship and to the Director of the Indian Institute of Science (Bangalore) for granting him a sabbatical leave. The assistance rendered by S. Sasidhara and R. Ravi, Department of Metallurgy, Indian Institute of Science, is gratefully acknowledged.

References

1. *Materials Properties Handbook: Titanium Alloys*, R. Boyer, G. Welsch, and E.W. Collings, eds., ASM International, Materials Park, OH, 1994, pp. 483-619.
2. R.W. Hertzberg: *Deformation and Fracture Mechanics of Engineering Materials*, 3rd ed., John Wiley Sons, New York, NY, 1987, p. 366.
3. S.R. Seagle, K.O. Yu, and S. Giangiordano: *Mater. Sci. Eng. A*, 1999, vol. A263, pp. 237-42.
4. D. Furrer: *Adv. Mater. Proc.*, 1999, No. 3, pp. 33-36.
5. S.L. Semiatin, V. Seetharaman, A.K. Ghosh, E.B. Shell, M.P. Simon, and P.N. Fagin: *Mater. Sci. Eng. A*, 1998, vol. A256, p. 92-110.
6. S.L. Semiatin, R.L. Goetz, E.B. Shell, V. Seetharaman, and A.K. Ghosh: *Metall. Mater. Trans. A*, 1999, vol. 30A, pp. 1411-24.
7. T. Seshacharyulu, S.C. Medeiros, J.C. Malas, W.G. Frazier, and Y.V.R.K. Prasad: "Microstructural Mechanisms during Hot Working of Commercial Grade Ti-6Al-4V with Lamellar Preform Structure," Wright-Patterson AFB, unpublished work, 1999.
8. T. Seshacharyulu, S.C. Medeiros, J.C. Morgan, J.C. Malas, W.G. Frazier, and Y.V.R.K. Prasad: *Mater. Sci. Eng. A*, 2000, vol. A279, pp. 289-99.
9. Y.V.R.K. Prasad, T. Seshacharyulu, S.C. Medeiros, J.C. Malas, and W.G. Frazier: *Mater. Sci. Technol.*, 2000, vol. 16, pp. 1029-36.
10. T. G. Nieh, J. Wadsworth, and O.D. Sherby: *Superplasticity in Metals and Ceramics*, Cambridge University Press, Cambridge, United Kingdom, 1997, p. 81.
11. A. Chaudhary, S.C. Medeiros, and J.C. Malas: Wright-Patterson AFB, unpublished work, 1997.
12. N. Ridley: *Superplasticity*, AGARD Lecture Series No. 168, NATO, France, pp. 4.1-4.14.
13. A.C.F. Cocks and M.F. Ashby: *Progr. Mater. Sci.*, 1982, vol. 27, pp. 189-244.
14. R. Raj: *Deformation Processing Maps*, Cornell University, Ithaca, NY, 1982.
15. *DEFORM User Manual*, Scientific Forming Technologies Corporation, Columbus, OH, 1998.